Nanoscale

PAPER

View Article Online
View Journal | View Issue

Cite this: *Nanoscale*, 2025, **17**, 25297

Effects of ethylenediamine on the intrinsic photoresponse of PbS quantum dots

Patrick Michel, Mario Martin, Jonas L. Hiller and Marcus Scheele *

We examine the intrinsic recombination dynamics of PbS quantum dots (QDs) functionalized with ethylenediamine (EDA) and compare it to that of the same QDs functionalized with ethane-1,2-dithiol (EDT). The recombination dynamics were studied as a function of temperature, pressure, and excitation intensity using asynchronous optical sampling (ASOPS). Only for EDA functionalization, we find that under vacuum at room temperature roughly 40% of the total photocurrent decays with a fast lifetime of approximately 100 picoseconds. Intensity-dependent studies indicate that the remaining recombination processes are consistent with trap-assisted Auger recombination mechanisms. Temperature-dependent measurements suggest that the fast 100 ps component is governed by a phonon-assisted decay process. Exploiting such processes could be beneficial for realizing GHz photodetection with PbS QDs.

Received 19th July 2025,
Accepted 9th October 2025

DOI: 10.1039/d5nr03057a

rsc.li/nanoscale

Introduction

As the demand for high-speed and energy-efficient nanoscale optoelectronic devices continues to grow, significant research efforts have been directed toward the development of novel materials capable of meeting these performance requirements.[1] Among other approaches, such as plasmonic antennas,[2] semiconductor nanoparticles—particularly lead sulfide quantum dots (PbS QDs)—have emerged as promising candidates due to their size-tunable optical properties[3] and high quantum efficiency.[4,5] PbS QDs are especially attractive for infrared photodetection, as they can be engineered to absorb at ≈1500 nm, a wavelength of relevance for applications in telecommunication, thermal imaging, and optical guidance systems. Their tunable bandgap[3] and compatibility with solution-based processing techniques provide distinct advantages over conventional bulk semiconductor materials in device fabrication. Despite these promising attributes, the role of the ligand shell in influencing the photodetector behaviour of PbS QDs remains insufficiently explored. Typically, the response time of a photodetector is assessed through extrinsic photocurrent measurements, which incorporate the influence of external factors such as device capacitance and carrier diffusion time, and has been found to be as short as 4 ns in PbS QDs.[6]

An alternative approach involves probing the intrinsic material properties—specifically, characteristics such as charge carrier recombination dynamics on the nanosecond timescale—which are governed solely by the material itself. These properties denote the fastest achievable times which the material can reach and are therefore relevant for estimation of the ultimate speed of the said material,[7,8] as well as providing insights into the material properties under exclusion of external limiting factors. To investigate this intrinsic behaviour, we synthesised PbS QDs with absorption peaks between 1520 nm and 1600 nm, to align it with the third telecom window. Fig. 1a presents the absorption spectra and first excitonic peaks of the selected nanoparticles. We attribute the additional peaks at approx. 1400 nm and 1750 nm for the PbS batch depicted in red to residual oleylamine from the synthesis of the particles.[9] In the past, hydrazine has been studied as a linker molecule between nanoparticles,[10,11] yielding good results when compared with a variety of different ligand systems. However, the volatility and toxicity of hydrazine are major drawbacks in its use. Therefore, we attempted to use a safer alternative and investigated the effect of the amine groups on the nanoparticle surface. We subsequently exchanged the native ligands with 1,2-ethylenediamine (EDA) or 1,2-ethanedithiol (EDT), employing EDT-functionalized QDs as a reference due to their well-documented properties in previous studies, notably by Maier *et al.*[12] A morphological analysis of the differently functionalized particles, shown in Fig. 1b, indicates differences in the film structure between the two ligand systems, with EDA often resulting in a more homogeneous coverage than EDT with a more clustered structure. (However, we note that film compositions vary between different samples as further described in the SI, section S2.)

The characterization of the intrinsic charge carrier dynamics in PbS nanoparticles was conducted using Asynchronous Optical Sampling (ASOPS), a two-pulse corre-

Institute of Physical and Theoretical Chemistry, University of Tübingen, Auf der Morgenstelle 18, 72076 Tübingen, Germany.
E-mail: marcus.scheele@uni-tuebingen.de

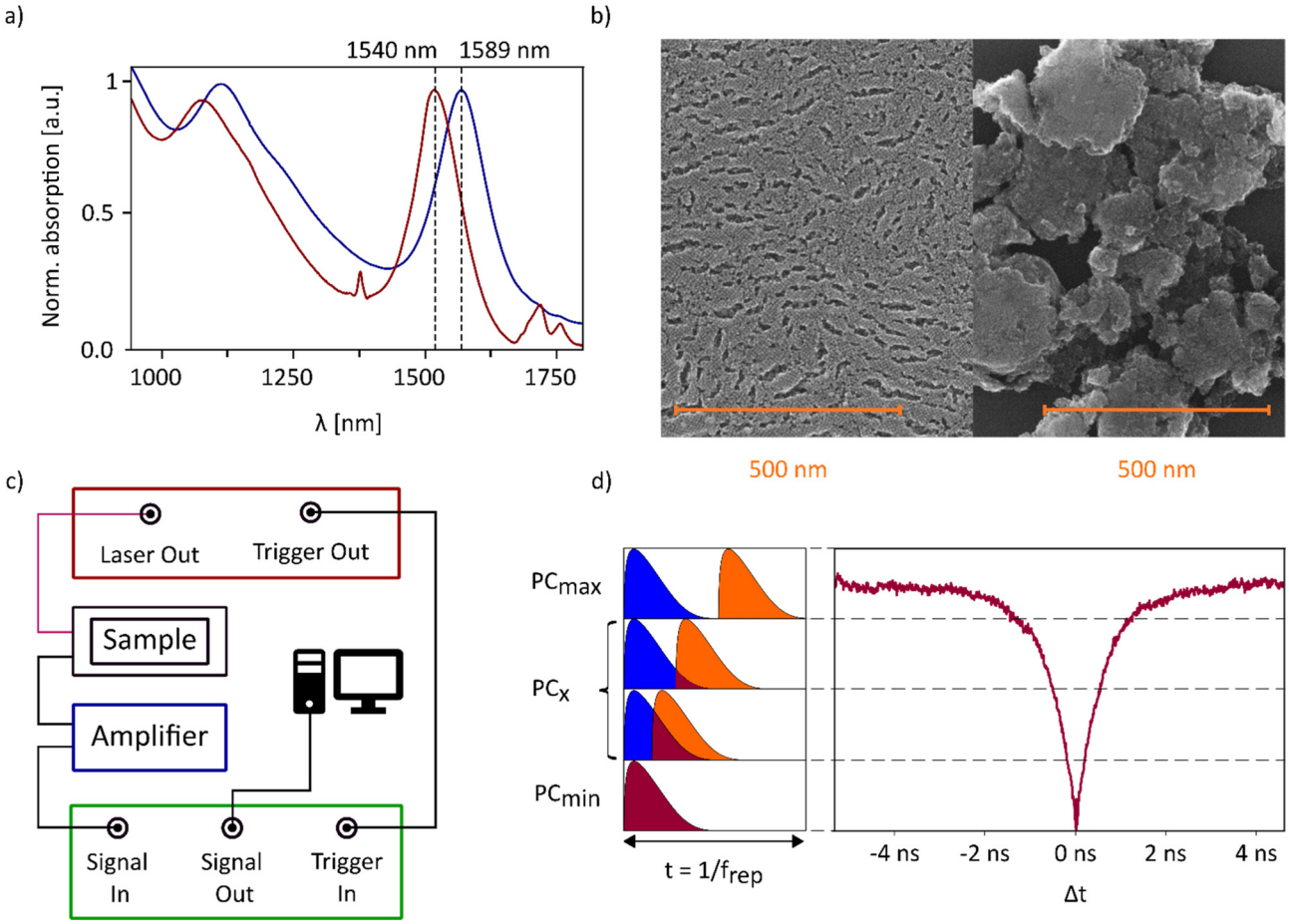

Fig. 1 (a) UV/Vis spectra of both batches of native PbS nanoparticles. (b) SEM images of PbS/EDA (left) and PbS/EDT (right) nanoparticle films. (c) Schematic depiction of the measurement setup. The ASOPS system (red) sends two laser pulses out to the sample (black) and these laser pulses are stacked *via* a beat frequency Δf, which is relayed to the lock-in (LI) amplifier (green). The laser pulse generates a photocurrent which is amplified *via* a transimpedance amplifier (blue) and further transmitted to the LI. (d) Working principle of the ASOPS system. Two laser pulses excite the material, resulting in a photocurrent that depends on the time delay between the pulses.

lation technique that enables ultrafast measurements on the nanosecond timescale with sub-picosecond temporal resolution. A schematic representation of the experimental setup is provided in Fig. 1c. The ASOPS system employs two cross-polarized pulsed lasers: one operating at a fixed repetition rate of 100 MHz and a second laser at 100 MHz minus a small delay frequency. In this study, the delay frequency ranged from 0.1 to 1 kHz. Importantly, variations in this delay frequency did not result in any observable material-dependent effects, indicating its robustness between different measurements. The delay frequency is used as the reference input for a lock-in amplifier, which synchronizes the data acquisition. Each data point is obtained over a 10 ns interval and separated by one pulse period of the laser, which ultimately limits the temporal resolution. The generated photocurrent signal is amplified using a transimpedance amplifier before being recorded by the lock-in system. Fig. 1d illustrates a typical measurement trace. A characteristic decay in the photocurrent is observed, attributed to the re-excitation of the system while slower components have not decayed, leading to an overall reduction in photocurrent. This decay curve is mirrored in the later half of the scan as the temporal order of the pump and probe pulses is reversed after full temporal overlap. For detailed technical specifications of the optical and electronic components utilized, refer to the SI (section S1).

Results

Exemplificative ASOPS measurements performed under a nitrogen atmosphere or vacuum for PbS/EDA and PbS/EDT are shown in Fig. 2. Under N_2, the recombination times of both systems behave identically with a mono-exponential decay of the photocurrent on the order of 1–2 ns. However, under vacuum the photocurrent decay of the EDA-functionalized particles can no longer be described with a single exponential function. Instead, fitting of the data requires a biexponential function, with the second component being on the order of approx. 100 ps. We observe this fast component for different PbS QD batches with different size distributions

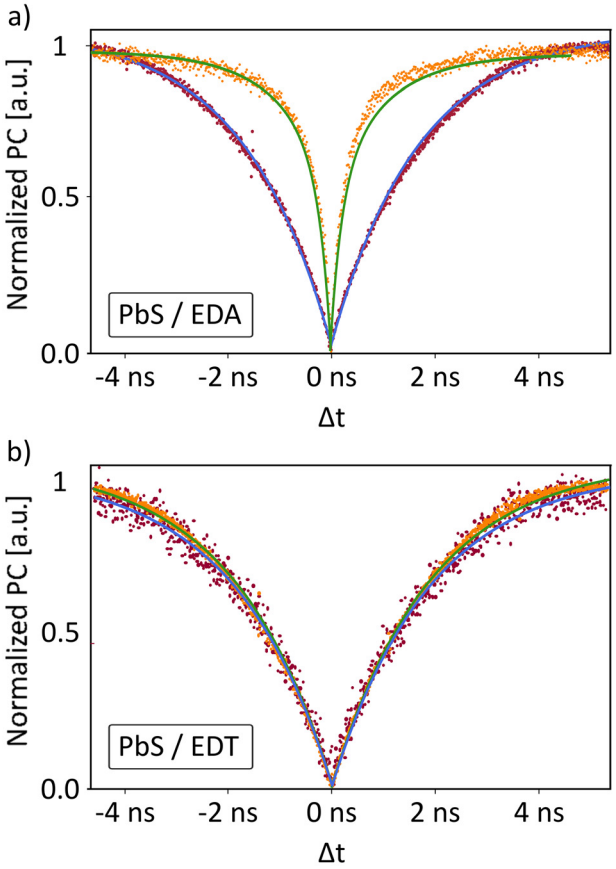

Fig. 2 Comparison of the intrinsic recombination times of functionalized PbS QDs under a nitrogen atmosphere and under vacuum. (a) PbS/EDA under vacuum (orange) and under N_2 (red), as well as the corresponding fits for the data in green and blue, respectively. (b) PbS/EDT under vacuum (orange) and under N_2 (red), as well as the corresponding fits for the data in green and blue, respectively.

(SI, section S3), while the photocurrent of the EDT-functionalized particles shows no pressure dependence.

A simple biexponential parallel decay model was used to fit the experimental data, as there was no evidence for the need of a more complex fit, such as the cascading decay model. The fitting function has the following form:

$$y(\Delta t) = A \times e^{-\frac{\Delta t}{\tau(1)}} + B \times e^{-\frac{\Delta t}{\tau(2)}} + c \quad (1)$$

Herein, A and B denote the relative contributions to the normalized photoresponse, Δt is the delay time between the two pulses of the ASOPS system, $\tau(n)$ is the decay time of the n-th exponential and c is the y-axis offset. A slight asymmetry at the theoretical $\Delta t = 0$ axis can be observed when looking at the fitted functions, which is especially noticeable in the PbS/EDA system under vacuum (Fig. 2a). This is likely a result of electromagnetic waves slightly modulating the signal, which does, however, not impact the results presented here (see the SI, section S3, for details).

We now investigate the effect of oxygen on the decay dynamics. To this end, the sample chamber was first evacuated, then flooded with N_2 and finally opened to the atmosphere. Overall, we observe a similar decay under vacuum and under ambient conditions (Fig. 3). Furthermore, the decay dynamics remain unchanged during continuous exposure to ambient conditions. We note, however, that there is a significant reduction in photocurrent over time under ambient conditions, reminiscent of particle degradation. No such effect is evident under vacuum conditions. A more detailed discussion of the degradation process is provided in section S3 of the SI.

To further concretize the potential decay pathways which result from the ligand exchange, we investigated the temperature dependence between 300 K and 200 K of these systems, shown in Fig. 4. On the right side of Fig. 4, semilogarithmic plots provide a visualisation of the different components in the measured decay times. PbS/EDT shows no change in decay time with varying temperatures, serving as a reference system (Fig. 4a–e). PbS/EDA, however, displays temperature dependent response times, especially between the temperatures of 300 K and 280 K, while the following temperature-dependent changes are smaller.

The most remarkable feature in PbS/EDA is the strong decrease of the relative contribution of the fast component in the fitting of the overall recombination process. This is further visualized in Fig. 4g–j where the data are plotted on a semilogarithmic scale by using the positive inverse of the data ($\Delta V_{max} - \Delta V$) and only the side with positive values for x ($\Delta t > 0$). The decrease of the contribution of the fast component resulting from a change of temperature can be observed when comparing Fig. 4h and j. In Fig. 4h, both components can be observed, as two linear fits are necessary to properly describe the data at 300 K, while one linear function is sufficient for the

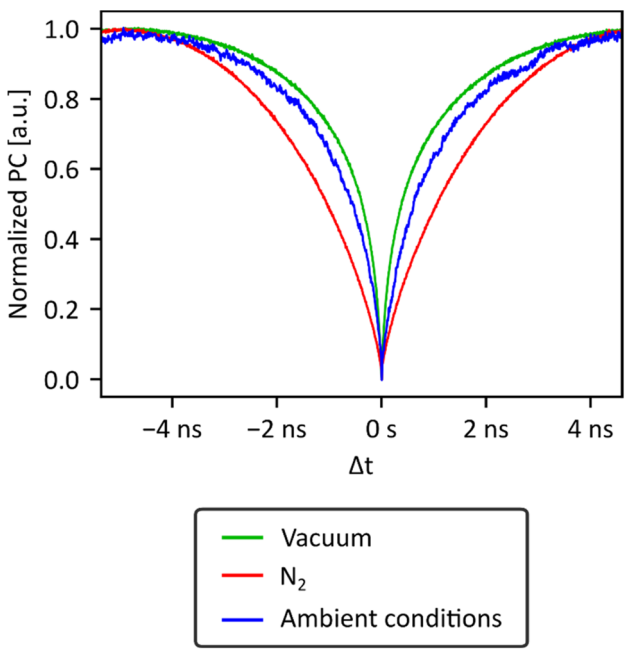

Fig. 3 Comparison of measurements performed under different environmental conditions.

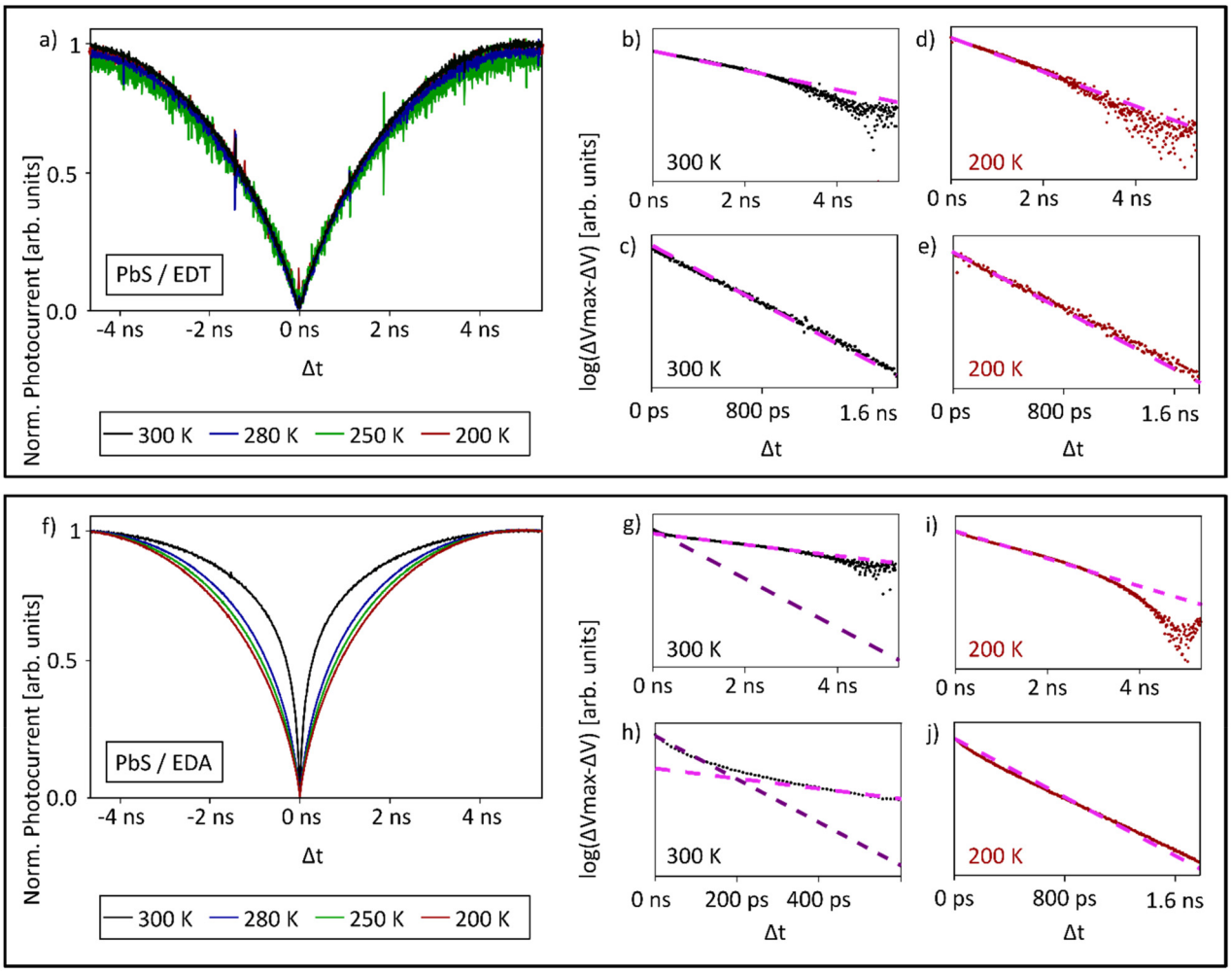

Fig. 4 Temperature dependence of PbS/EDA and PbS/EDT from 300 K to 200 K. (a) ASOPS measurements of PbS/EDT at different temperatures. (b and g) Semilogarithmic plot of the measurements at 300 K for $\Delta t > 0$. A linear function (pink) is included as a visual aid. (c) Magnification of the data presented in (b), from 0 to 1.7 ns. (d) Semilogarithmic plot of the measurements at 200 K and magnification of the data in the region from 0 to 1.7 ns (e). (f) ASOPS measurements of PbS/EDA at different temperatures. (h) Magnification of the data presented in (g), from 0 to 500 ps, showing the area in which the two linear functions were inserted to exemplify the two components. (i) Semilogarithmic plot of the measurements at 200 K and magnification of the data in the region from 0 to 1.6 ns (j).

measurements at 200 K (Fig. 4j). This highlights the difference between the two functionalizations, when comparing those plots with the corresponding measurements for PbS/EDT (Fig. 4c and e).

For a robust statistical analysis of the temperature-dependent data, the dataset was investigated *via* random sampling with replacement. Through this method, we observe a continuous increase in the slow response time τ_1 from 1.4 ns (300 K) to 1.8 ns (200 K) while the fast response time τ_2 shows varying times between 138 ps and 214 ps, without a clear trend. The changes in the times are, however, comparatively small when compared to the contribution of the amplitude of the second component, which is represented by parameter "*B*" in eqn (1). The contribution of the fast component to the overall function changes from 42.6% at 300 K to 9.3% at 200 K, making this the most important trend. The importance of the amplitudes of the functions is further exemplified by the variance of τ_2 across different measurements. Herein, the 214 ps presented in Fig. 4 is one of the slowest measured response times for this effect while the response time presented in Fig. 5 is among the fastest (60 ps). The changes in actual response times and the correlation with the amplitude of the fitting functions are further detailed in sections S4 and S5 of the SI and an overview of different response times across a variety of measurements is provided in section S6.

In order to study the influence of charge carrier generation on the response times, laser-intensity dependent measurements are performed on both EDA and EDT exchanged QDs, displayed in Fig. 5. Attenuators are used in the form of dB filters to reduce the excitation power to 50% (3 dB) and 10% (10 dB) intensity. For both measurements, the decay time of the slow component changes, while in the PbS/EDA measurements the fast component remains constant. The corresponding values obtained during these measurements are displayed in Table 1

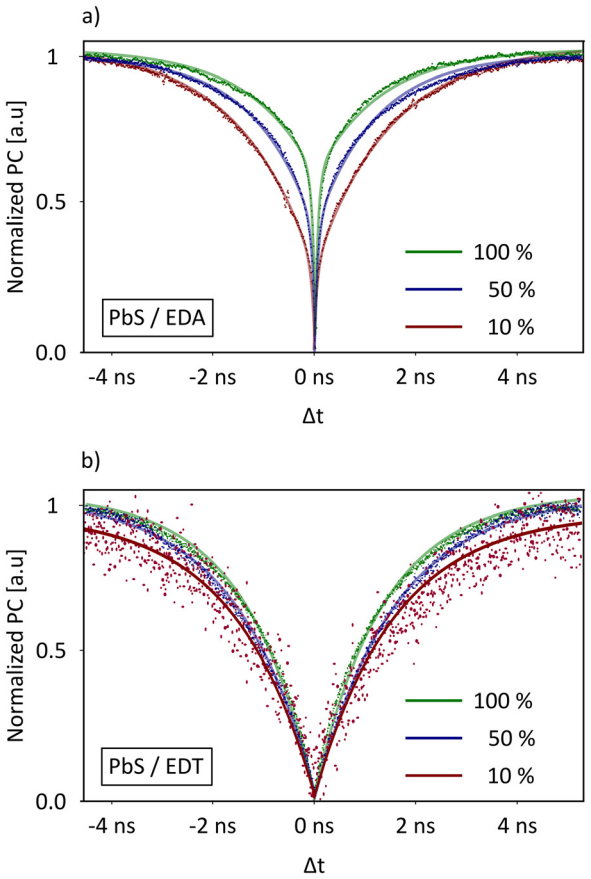

Fig. 5 Intensity-modulated ASOPS measurements for PbS/EDA (a) and PbS/EDT (b).

Table 1 Recombination times for ASOPS measurements performed at different laser powers (100%, 50% and 10%). The two components required for the PbS/EDA measurements are represented as τ_1 and τ_2. For the EDT exchanged QDs, a single recombination time is sufficient

		Laser power		
		100%	50%	10%
EDA	$\lvert\tau_1\rvert$	1.40 ns	1.45 ns	1.60 ns
	$\lvert\tau_2\rvert$	60 ps	60 ps	60 ps
EDT	$\lvert\tau\rvert$	1.40 ns	1.50 ns	1.60 ns

Discussion

We attempt a discussion of the observed intrinsic recombination processes in the framework of three mechanisms, which have been shown to be relevant for colloidal and 2D materials in previous reports: trap assisted recombination,[13–16] hot carrier cooling[14,17,18] and phonon assisted recombination.[13,16,19,20]

Both PbS/EDT and PbS/EDA show a relatively slow recombination component (associated with τ_1) on the order of 1–2 ns, which increases marginally with decreasing temperature and irradiance. Trap assisted recombination mechanisms have been previously reported for PbS/EDT by Maier *et al.*[12] More specifically, one has to distinguish between the Shockley–Reed–Hall mechanism and the trap assisted Auger mechanism (TAA) as possible recombination processes involving interband trap states. In that work, the excitation power-dependence of the response time was taken as supporting evidence that the dominant mechanism in PbS/EDT is TAA, as it is dependent on the carrier density, and therefore on the power of the excitation laser.[12,21–23] Since we observe a similar power-dependence for both systems shown in Fig. 5, PbS/EDT and PbS/EDA, we reason that TAA is the mechanism responsible for the slow recombination process τ_1.

From here on we focus on the second component τ_2, which is observable under vacuum and ambient conditions for PbS/EDA, and try to find the most plausible mechanism based on the obtained data. Hot carrier cooling has previously been shown to lead to recombination times as fast as 1.5 ps in graphene,[24] and a few ps in WS_2,[25] measured with pump–probe photocurrent dependent measurements and transient absorption, respectively. While the timescales of these recombination processes are comparable to our own findings, the temperature dependence of the PbS/EDA system does not match the results in graphene published by Sun *et al.*[24] In that work, the changes in the response times were observed over the entire temperature range from 20 K to 298 K, contrasting our findings in Fig. 4 that below 250 K, τ_2 remains constant. Brown *et al.* have compared the electronic properties of PbS QDs exchanged with EDT *vs.* EDA,[26] and from that work it is not obvious why the efficiency of hot carrier harvesting should vary significantly between the two materials. Furthermore, we observe τ_2 only under vacuum or ambient conditions, suggesting either the role of some form of ligand stripping from the QDs or the introduction of additional trap or defect states due to the interaction with air. This would be in line with the generally weaker binding strength of amines *vs.* thiols on PbS,[27–30] allowing for the desorption of the ligands under vacuum or replacement with O_2/H_2O. However, to our knowledge, no direct correlation between free surfaces and hot carrier cooling has been found. We therefore suspect that the cooling of hot carriers, assisted *via* optical phonons, is not a main contributor to the electronic recombination in our system, mainly due to a disparity in the timescales when compared to graphene where it has been shown to occur within a few picoseconds.[31–33] Indeed, follow-up measurements on the PbS/EDA system on a timescale of a few picoseconds have shown weak additional dynamics that can be interpreted as hot carrier cooling. However, due to its weak amplitude, this signal was not further investigated (see section S3 of the SI for further information.)

We thus return to discussing the provenance of the ~100 ps component. Phonon assisted recombination has been investigated with several QD materials using a variety of different methods[34–36] and the increased effects of phonon assisted decay mechanisms at higher temperatures in QD systems have been previously calculated.[35] Further calculations show that surface ligands have a major influence on the QD system,[34]

which matches the previously reported similar surface energies of both EDA and EDT systems.[37] This is in line with our observation that under N_2 both EDA and EDT exchanged QDs behave nearly identically.

The different behaviour observed under vacuum must therefore be attributed to changes in the QD/ligand system, which in our view supports the hypothesis that ligand removal from the QD surface generates free surface states. Before proceeding with a mechanistic discussion of the 100 ps component, the fact that the system behaves identically under both vacuum and ambient conditions warrants further consideration. One possible explanation would be that additional trap states due to hydroxyl groups[27] as a result of the exposure to atmospheric conditions could lead to the second decay component. We further attempted sample transfer under inert conditions, limiting exposure to oxygen as much as possible, and found no difference compared to samples briefly exposed to air. More details about these studies are provided in section S3 of the SI.

This leaves open the question of why N_2 specifically suppresses the second decay component, a phenomenon we are unable to explain at present. Nevertheless, one observation that supports our hypothesis of phonon-assisted recombination, apart from the previously described I_{ilum} measurements, is the distinct temperature dependence of the process. Future studies, employing *e.g.* wavelength-dependent excitation of phonon modes, could shed more light on this question.[38]

Generally, electron–phonon induced Auger processes are temperature-dependent. They have been described to show ln (T/T_0),[34] dependence, but also other temperature correlations have been described, especially considering the different approaches to phonon assisted carrier cooling with regard to the influence of electron- and lattice-temperatures of the material.[35,39–41] Similar observations made in graphene that involve acoustic phonons support our attribution to a phonon-assisted cooling mechanism.[31,33] However, in view of the substantial differences between the two materials, this comparison would benefit from theoretical calculations to substantiate it further. In contrast, if the decay was trap-induced and assisted by oxygen, temperature dependence would only be expected in the case of very shallow trap states. The energy difference between 298 K and 250 K corresponds to approximately 4 meV, which would allow for re-excitation processes to occur at room temperature.

Taking all these points into consideration, we hold (acoustic) phonon assisted recombination to be the most plausible cause for the fast τ_2 component. Future material design with the objective of enabling sub-ns photoresponse times should therefore focus on emphasizing phonon-assisted recombination in PbS QDs, especially under ambient conditions. With the PbS/EDA system, a substantial fraction of the recombination dynamics can be attributed to this effect at 300 K, making it suitable for future investigation as a GHz photodetector. However, the current need for operation under vacuum and the degradation under atmospheric influences are obvious technological drawbacks.

Conclusions

We performed intrinsic photocurrent measurements on ethylenediamine (EDA)- and 1,2-ethanedithiol (EDT)-exchanged PbS quantum dots. Under both vacuum and ambient conditions, the EDA-exchanged particles show a faster, second decay component on the order of 100 ps, which is not present in the EDT-exchanged particles. Our experiments provide evidence that the most likely mechanism for this fast recombination is phonon assisted recombination. Such sub-nanosecond photoresponse provides exciting prospects for GHz photodetection with PbS quantum dots, especially if the current limited long-term stability under ambient conditions could be overcome in the future.

Experimental

Synthesis of PbS-nanocrystals

The synthesis of PbS nanoparticles was performed following a procedure adapted from Weidman *et al.*[3] The sulphur precursor was prepared by dissolving 80 mg of elemental sulphur (Acros Organics, 99.9%) in 7.5 mL of oleylamine (Thermo Scientific, 80–90%) (OLA), followed by stirring at 100 °C for 2 hours under an inert nitrogen atmosphere. Separately, 5.0 g of lead(II) chloride (Thermo Scientific, 99%) ($PbCl_2$) was dispersed in 15 mL of oleylamine and subjected to degassing at 120 °C for 2 hours to remove residual oxygen and moisture. The solution was then purged with nitrogen to ensure an inert environment. The sulphur precursor was subsequently heated to 120 °C, and 2.25 mL of the hot sulphur precursor was rapidly injected into the $PbCl_2$/OLA solution under inert conditions. The reaction was allowed to proceed for 6 minutes and 30 seconds before being quenched by the addition of 20 mL of ice-cooled *n*-hexane (Thermo Scientific, >97%, extra dry) and immediate immersion in an ice bath. The resulting dispersion was transferred to a nitrogen-filled glovebox and stirred with 10 mL of oleic acid (Thermo Scientific, 90%) for 30 minutes to improve colloidal stability. Nanoparticles were isolated by adding ethanol (Thermo Scientific, >99.5%, extra dry) in a 1 : 1 volume ratio with respect to the reaction mixture, followed by centrifugation at 4000 rpm for 10 minutes. The supernatant was discarded, and the precipitate was redispersed in *n*-hexane. This purification process was repeated twice to remove excess ligands and $PbCl_2$ left in the reaction mixture. The final product was redispersed in approximately 6 mL of *n*-hexane for storage.

Optical characterization

Optical characterization of the PbS-QDs was carried out using a Cary 5000 UV-Vis-NIR spectrophotometer (Agilent Technologies). A volume of 100 μL of the PbS stock solution in hexane was deposited in an open glass vial and allowed to evaporate under inert conditions. It is important to note that the application of vacuum to accelerate the drying process significantly decreased the solubility of the QDs. Following

solvent evaporation, the dried QDs were re-dissolved in 3 mL of tetrachloroethylene (Fisher Scientific, ≥99% purity) under ambient conditions. The resulting dispersion was transferred to a standard optical cuvette, and absorption spectra were recorded in the range of 900–1800 nm. Pure tetrachloroethylene was used as the reference baseline for all spectral measurements.

Optical lithography

We used optical lithography to fabricate the required substrates for our measurements. Silicon wafers (15 × 15 mm) with a silicon dioxide layer of approximately 770 nm thickness were utilized. Prior to processing, the substrates were cleaned with acetone and isopropanol. Afterwards, 80 μL of a negative photoresist (ma-N 405, Microresist Technology) was spin-coated onto the substrates at 3000 rpm for 30 seconds. The coated substrates were then baked on a hotplate at 100 °C for 1 minute. Following this, the substrates were aligned and exposed to UV light through a photomask, using a mask aligner to etch the desired electrode pattern. The exposed substrates were afterwards developed by immersion in ma-D 331/S developer (Microresist Technology) for approximately 4 minutes. The samples were then rinsed twice with ultrapure water (Milli-Q) to remove any residual developer. A thin metal layer was evaporated in a vacuum chamber, consisting of 2 nm titanium followed by 20 nm gold. The titanium layer served as an adhesion promoter for the gold. Finally, the lift-off process was performed by immersing the substrates in acetone within an ultrasonic bath for approx. 1 min, followed by a cleaning step with isopropanol to remove any remaining photoresist.

Ligand exchange

The ligand exchange process was performed directly on the substrate, following a protocol adapted from Maier *et al.*[12] All steps were performed inside a glovebox. First 75 μL of a PbS-QD solution in hexane (5 μM) was deposited onto a silicon substrate and spin-coated at 3000 rpm for 30 seconds to form a QD film. Subsequently, 150 μL of a ligand solution—either 5 mM 1,2-ethanedithiol (EDT) in acetonitrile or 5 mM ethylenediamine (EDA) in methanol—was applied to the QD-coated substrate. After allowing the solution to interact with the film for 30 seconds, the sample was again spin-coated with the same parameters. The substrate was then washed with the corresponding solvent (acetonitrile for EDT and methanol for EDA) to remove excess ligands. This ligand exchange procedure was repeated twice for each sample to ensure complete surface coverage. Upon completion, the samples were stored under inert conditions.

Optoelectrical measurements

Both intrinsic and extrinsic measurements were conducted using a LakeShore Cryotronics CRX-6.5 K probe station under inert conditions. The sample was initially loaded into the probe station under ambient conditions, after which the chamber was evacuated for approximately 20 minutes and subsequently filled with nitrogen. Intrinsic photoresponse measurements were performed using an optical sampling engine (Menlo Systems) in combination with an integrated combiner box. The cross-polarized lasers were coupled into an optical fibre and introduced into the probe station, where the sample was illuminated without further focusing to ensure uniform excitation across the entire measured channel. A similar procedure was employed for extrinsic measurements, where picosecond pulsed lasers with emission wavelengths of 636 nm and 780 nm were used (PicoQuant; Taiko PDL M1 (controller), LHD Series (laser sources), 780 nm and 636 nm). These sources were also fibre-coupled and delivered to the sample within the probe station.

Author contributions

M. S. initiated, supervised and secured funding for the project. M. M. performed and evaluated the extrinsic measurements. P. M. synthesized and characterized the PbS nanocrystals, planned and performed the intrinsic ASOPS Measurements as well as the data analysis. Robustness analysis of the data was performed by J. L. H. and P. M. The manuscript was written by M. S. and P. M. with input from all authors.

Conflicts of interest

There are no conflicts to declare.

Data availability

The data supporting this article have been included as part of the supplementary information (SI). Supplementary information: supporting measurements, random sampling with replacement analysis, confirmation of signal validity, and SEM images. See DOI: https://doi.org/10.1039/d5nr03057a.

Acknowledgements

Financial support of this work has been provided by the Deutsche Forschungsgemeinschaft (DFG) under grant SCHE1905/9-1 (project no. 426008387). SEM measurements were performed by Elke Nadler (University of Tübingen). We thank Fabian Strauß for performing additional extrinsic measurements.

References

1 J. He, C. Huang, H. Wen, X. Wang, Y. He and Y. Dan, *Nanotechnology*, 2020, **31**, 195201.
2 H. Siampour and Y. Dan, *Opt. Express*, 2016, **24**, 4601.
3 M. C. Weidman, M. E. Beck, R. S. Hoffman, F. Prins and W. A. Tisdale, *ACS Nano*, 2014, **8**, 6363–6371.
4 R. Saran and R. J. Curry, *Nat. Photonics*, 2016, **10**, 81–92.

5 Q. Xu, L. Meng, K. Sinha, F. I. Chowdhury, J. Hu and X. Wang, *ACS Photonics*, 2020, **7**, 1297–1303.
6 Y. Deng, C. Pang, E. Kheradmand, J. Leemans, J. Bai, M. Minjauw, J. Liu, K. Molkens, J. Beeckman, C. Detavernier, P. Geiregat, D. Van Thourhout and Z. Hens, *Adv. Mater.*, 2024, **36**, 2402002.
7 T. F. Carruthers and J. F. Weller, *Appl. Phys. Lett.*, 1986, **48**, 460–462.
8 A. Urich, K. Unterrainer and T. Mueller, *Nano Lett.*, 2011, **11**, 2804–2808.
9 D. Baranov, M. J. Lynch, A. C. Curtis, A. R. Carollo, C. R. Douglass, A. M. Mateo-Tejada and D. M. Jonas, *Chem. Mater.*, 2019, **31**, 1223–1230.
10 S. J. Kim, W. J. Kim, Y. Sahoo, A. N. Cartwright and P. N. Prasad, *Appl. Phys. Lett.*, 2008, **92**, 031107.
11 O. E. Semonin, J. M. Luther, S. Choi, H.-Y. Chen, J. Gao, A. J. Nozik and M. C. Beard, *Science*, 2011, **334**, 1530–1533.
12 A. Maier, F. Strauß, P. Kohlschreiber, C. Schedel, K. Braun and M. Scheele, *Nano Lett.*, 2022, **22**, 2809–2816.
13 A. P. Frauendorf, A. Niebur, D. Rudolph, M. Oestreich, J. Lauth and J. Hübner, *J. Phys. Chem. C*, 2024, **128**, 16597–16606.
14 J. M. Empey, C. Grieco, N. W. Pettinger and B. Kohler, *J. Phys. Chem. C*, 2021, **125**, 14827–14835.
15 N. Ganesh, A. Ghorai, S. Krishnamurthy, S. Banerjee, K. L. Narasimhan, S. B. Ogale and K. S. Narayan, *Phys. Rev. Mater.*, 2020, **4**, 084602.
16 Y. Kobayashi and N. Tamai, *J. Phys. Chem. C*, 2010, **114**, 17550–17556.
17 I. Nadinov, K. Almasabi, L. Gutiérrez-Arzaluz, S. Thomas, B. E. Hasanov, O. M. Bakr, H. N. Alshareef and O. F. Mohammed, *ACS Cent. Sci.*, 2024, **10**, 43–53.
18 C. Burda, X. Chen, R. Narayanan and M. A. El-Sayed, *Chem. Rev.*, 2005, **105**, 1025–1102.
19 M. Karakus, S. A. Jensen, F. D'Angelo, D. Turchinovich, M. Bonn and E. Cánovas, *J. Phys. Chem. Lett.*, 2015, **6**, 4991–4996.
20 P. Lugli and S. M. Goodnick, *Phys. Rev. Lett.*, 1987, **59**, 716–719.
21 V. I. Klimov, A. A. Mikhailovsky, D. W. McBranch, C. A. Leatherdale and M. G. Bawendi, *Phys. Rev. B: Condens. Matter Mater. Phys.*, 2000, **61**, R13349–R13352.
22 T. Nishihara, H. Tahara, M. Okano, M. Ono and Y. Kanemitsu, *J. Phys. Chem. Lett.*, 2015, **6**, 1327–1332.
23 H. Wang, C. Zhang and F. Rana, *Nano Lett.*, 2015, **15**, 339–345.
24 D. Sun, G. Aivazian, A. M. Jones, J. S. Ross, W. Yao, D. Cobden and X. Xu, *Nat. Nanotechnol.*, 2012, **7**, 114–118.
25 T. Wang, T. R. Hopper, N. Mondal, S. Liu, C. Yao, X. Zheng, F. Torrisi and A. A. Bakulin, *ACS Nano*, 2023, **17**, 6330–6340.
26 P. R. Brown, D. Kim, R. R. Lunt, N. Zhao, M. G. Bawendi, J. C. Grossman and V. Bulović, *ACS Nano*, 2014, **8**, 5863–5872.
27 M. Gu, Y. Wang, F. Yang, K. Lu, Y. Xue, T. Wu, H. Fang, S. Zhou, Y. Zhang, X. Ling, Y. Xu, F. Li, J. Yuan, M. A. Loi, Z. Liu and W. Ma, *J. Mater. Chem. A*, 2019, **7**, 15951–15959.
28 J. Xu, O. Voznyy, M. Liu, A. R. Kirmani, G. Walters, R. Munir, M. Abdelsamie, A. H. Proppe, A. Sarkar, F. Pelayo García De Arquer, M. Wei, B. Sun, M. Liu, O. Ouellette, R. Quintero-Bermudez, J. Li, J. Fan, L. Quan, P. Todorovic, H. Tan, S. Hoogland, S. O. Kelley, M. Stefik, A. Amassian and E. H. Sargent, *Nat. Nanotechnol.*, 2018, **13**, 456–462.
29 D. Bederak, N. Sukharevska, S. Kahmann, M. Abdu-Aguye, H. Duim, D. N. Dirin, M. V. Kovalenko, G. Portale and M. A. Loi, *ACS Appl. Mater. Interfaces*, 2020, **12**, 52959–52966.
30 J. M. Luther, M. Law, Q. Song, C. L. Perkins, M. C. Beard and A. J. Nozik, *ACS Nano*, 2008, **2**, 271–280.
31 D. Sun, Z.-K. Wu, C. Divin, X. Li, C. Berger, W. A. De Heer, P. N. First and T. B. Norris, *Phys. Rev. Lett.*, 2008, **101**, 157402.
32 R. Bistritzer and A. H. MacDonald, *Phys. Rev. Lett.*, 2009, **102**, 206410.
33 S. Butscher, F. Milde, M. Hirtschulz, E. Malić and A. Knorr, *Appl. Phys. Lett.*, 2007, **91**, 203103.
34 K. Hyeon-Deuk, Y. Kobayashi and N. Tamai, *J. Phys. Chem. Lett.*, 2014, **5**, 99–105.
35 A. Grodecka-Grad and J. Förstner, *J. Phys.: Conf. Ser.*, 2010, **245**, 012035.
36 E. R. Kennehan, K. T. Munson, C. Grieco, G. S. Doucette, A. R. Marshall, M. C. Beard and J. B. Asbury, *J. Phys. Chem. C*, 2021, **125**, 22622–22629.
37 P. R. Brown, D. Kim, R. R. Lunt, N. Zhao, M. G. Bawendi, J. C. Grossman and V. Bulović, *ACS Nano*, 2014, **8**, 5863–5872.
38 H. Siampour, C. O'Rourke, A. J. Brash, M. N. Makhonin, R. Dost, D. J. Hallett, E. Clarke, P. K. Patil, M. S. Skolnick and A. M. Fox, *npj Quantum Inf.*, 2023, **9**, 15.
39 T. Low, V. Perebeinos, R. Kim, M. Freitag and P. Avouris, *Phys. Rev. B: Condens. Matter Mater. Phys.*, 2012, **86**, 045413.
40 V. A. Belyakov, V. A. Burdov, D. M. Gaponova, A. N. Mikhaylov, D. I. Tetelbaum and S. A. Trushin, *Phys. Solid State*, 2004, **46**, 27–31.
41 Ł. Dusanowski, A. Musiał, G. Sęk and P. Machnikowski, *Acta Phys. Pol., A*, 2013, **124**, 813–816.

